Journal of The Electrochemical Society, **159** (10) A1730-A1738 (2012)
0013-4651/2012/159(10)/A1730/9/$28.00 © The Electrochemical Society

Battery Cycle Life Prediction with Coupled Chemical Degradation and Fatigue Mechanics

Rutooj Deshpande,[a,z] Mark Verbrugge,[b,*] Yang-Tse Cheng,[a,*] John Wang,[c,*] and Ping Liu[c,*]

[a] *Chemical and Materials Engineering, University of Kentucky, Lexington, Kentucky 40506, USA*
[b] *General Motors Global R&D Center, Warren, Michigan 48090, USA*
[c] *HRL Laboratories LLC, Malibu, California 90265-4797, USA*

Coupled mechanical-chemical degradation of electrodes upon charging and discharging has been recognized as a major failure mechanism in lithium ion batteries. The instability of commonly employed electrolytes results in solid electrolyte interphase (SEI) formation. Although the SEI layer is necessary, as it passivates the electrode-electrolyte interface from further solvent decomposition, SEI formation consumes lithium and thus contributes to irreversible capacity loss. In this paper, we study irreversible capacity loss in a graphite-$LiFePO_4$ cell. Our results support the mechanism of irreversible capacity loss due to the consumption of lithium in forming SEI. We attribute irreversible capacity loss to diffusion induced stresses (DISs) that cause pre-existing cracks on the electrode surfaces to grow gradually upon cycling, leading to the growth of SEI on the newly exposed electrode surfaces. Because lithium is consumed in forming the new SEI, irreversible capacity loss continues with cycling. Along with the SEI formation upon newly exposed (cracked) surfaces, the existing SEI thickness also grows with cycling, resulting in additional loss of lithium. In this study, we provide, a simple mathematical model, based on the Paris' Law formulation of mechanical fatigue, in combination with chemical degradation to explain battery life. We compare the predicted capacity at different temperatures with the experimental data obtained from electrochemical measurements on graphite-$LiFePO_4$ cells.
 [DOI: 10.1149/2.049210jes]

Manuscript submitted April 23, 2012; revised manuscript received July 19, 2012. Published August 29, 2012.

The cycle life prediction of the commercial lithium ion batteries is of intense interest for many applications, including demanding traction applications. Battery capacity decays upon electrochemical cycling as a result of several degradation mechanisms, such as irreversible lithium loss due to solid electrolyte interphase (SEI) formation, particle cracking, particle isolation, etc. Among these degradation mechanisms, the chemical degradation, as a result of solvent reduction by lithium, which can lead to SEI formation, has been widely recognized as a major cause of loss of active lithium.[1–5] The 'Calendar life' of a battery is associated with chemical degradation. Spotnitz et al.[6] reviewed capacity fading measurements and models for predicting the calendar life of lithium ion batteries. While some of the models, such as that of Bloom et al.,[7] are semi-empirical, others such as that of Christensen and Newman,[8] consider chemical degradation as a major source of capacity fading and thus predict the calendar life of the battery.[8–15] Broussely et al.[16] measured capacity loss of batteries at several temperatures and put forward a mathematical model which predicts calendar life. Ning et al.[17] developed a computer simulation model based on solvent reduction at the electrode-electrolyte interface as a major source of lithium loss. Safari et al.[9,10] proposed a methodology derived from the mechanical-fatigue theory to predict the life of a Li-ion battery, assuming that the source of aging is the growth of SEI at the anode. Ramadass et al.[18] developed a capacity fade prediction model for Li-ion cells based on a semi-empirical approach. Santhanagopalan et al.[19] have reviewed various life prediction models. Along with chemical degradation, mechanical degradation is also a major aspect of capacity fading that is often ignored in published life prediction models. Mechanical degradation can be caused by diffusion induced stresses as a result of volume changes during charging and discharging the battery. There have been several articles published in the literature that discuss mechanical stresses in single electrode particles and experimental observation of DISs in thin films.[20–24] Through mathematical modeling, we recently investigated the effects of operating conditions, electrode particle size, particle shape, and phase transformation on DISs in electrodes.[25–29] In this paper, we couple mechanical degradation with chemical degradation to develop an initial approach to understand battery life.

$LiFePO_4$ based cells are promising candidates for large scale applications in the automotive industry because of their excellent chemical and thermal stability and potential for low cost.[30–34] Liu et al.[35] established lithium loss as a major mechanism for capacity fading of this system and presented a semi-empirical model for life cycle prediction.[36] A robust phenomenological life model to describe the physics behind capacity fading is still required to predict cell life over a characteristic cycling protocol and to establish a rational accelerated life test. Here, with cycling experiments and modeling results, we find that lithium loss is consistent with our destructive physical diagnoses after cycling and with our non-destructive electrochemical analyzes during cycling of the graphite-$LiFePO_4$ cells.

Specifically, in this work, we cycle graphite-$LiFePO_4$ cells at different temperatures under potentiostatic and galvanostatic operation. We monitor the capacity fade as a function of the number of cycles. We propose a mathematical model to describe the lithium loss caused by coupled chemical and mechanical degradation. We find that the model describes the battery life with good accuracy; that is, the difference between the model and experimental results is similar in magnitude to the differences between experimental data sets. In addition, we model the voltage curves for the battery at different cycles and find favorable agreement with the experimental voltage curves. We further determine individual electrode potentials, which contribute to the total cell voltage, to understand the individual electrode behavior with cycling. The model we develop is closely related to the discussion and schematic illustrations provided by Wachtler, Besenhard, and Winter.[3] These authors outline in detail various mechanisms that lead to irreversible capacity losses and compare and contrast the degradation phenomena occurring at carbonaceous electrode surfaces with those of lithium storage metals and alloys. From a modeling perspective, to our knowledge this is the first attempt to couple chemical degradation with mechanical degradation (i.e., a crack propagation model driven by diffusion induced stress and subsequent lithium-consuming passivation reactions over new crack surfaces) for the capacity loss prediction. While the theory we propose is rudimentary, and the experiment-theory comparison is conducted over a range of rather modest current densities (consistent with electric vehicle applications, versus, for example, higher current densities seen in conventional hybrid electric vehicle applications), this work does highlight phenomena that must be more fully understood to improve our ability to understand how lithium ion batteries degrade.

Theoretical Background

We assume that the electrode consists of a large number of spherical graphite particles of uniform size. Freshly exposed surfaces give rise to SEI formation during the subsequent charge due to electrolyte reduction in the presence of high lithium contents within the carbon

*Electrochemical Society Active Member.
[z] E-mail: rutooj.deshpande@uky.edu

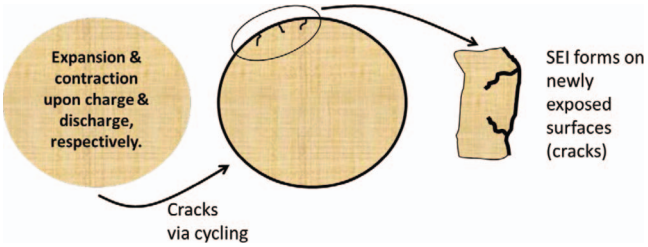

Figure 1. A cartoon diagram representing the schematics of the lithium loss as proposed. As a result of diffusion induced stresses (DISs), the cracks at the particle surface propagate with cycling, new surface is exposed to electrolyte, and Li is consumed in the formation of new SEI.

host. For example, the ethylene carbonate solvent can be reduced in the presence of lithiated carbon[2]

$$2[\text{Li-S}] + 2e^- + \text{EC} \longrightarrow \text{Li}_2\text{CO}_3 + \text{H}_2\text{C}{=}\text{CH}_2 + 2\text{S}$$

where lithium guest species corresponds to [Li-S] and S is a vacant site within the host carbon.[37] The lithium carbonate product leads to SEI formation, stabilization of the exposed electrode surface, and a loss of lithium from the cell. We assume that the newly exposed surface is covered by SEI over the subsequent charge cycle, as described above chemical reaction. We note this is an approximation and that the SEI may be a complex mixture of many solid phases; one could generalize the model to comprehend a multiphase, multispecies SEI should sufficient data become available for the respective species and phases. Last, as will be discussed, we assume that the existing SEI grows in thickness with time.

As a result of the DISs, the cracks at the particle surface propagate upon electrochemical cycling. For each cycle, the newly cracked surface is exposed to electrolyte and thus results in SEI formation. Fig. 1 provides a schematic illustration of the lithium loss mechanism leading to capacity decline.

Experimental

The commercially available 2.2 Ah, 28650 cylindrical cells were purchased from A123 Systems. The electrodes are a $LiFePO_4$ cathode (positive) and a carbon (substantially graphitic) anode (negative); hence, we shall refer to these as C-LFP cells. These lithium-ion cells were tested at three different temperatures (15, 45, 60°C). For all tests, the cell current was maintained at C/2 (for both charge and discharge), and the cells were fully charged and subsequently discharged to 90% depth of discharge (DOD). In defining the DOD and C rates, the cell is de-rated to 2 Ah. Consequently, C rate corresponds to a current of 2 A. The cutoff voltages for the cycle test of all the cells were at 3.6 V and 2.0 V. The cells were charged to 3.6 V and held at 3.6 V until the current dropped below 0.1A for a maximum of 2 days. Prior to cycling tests, each cell was characterized using these four techniques: 1) capacity characterization, 2) relaxation test, 3) electrochemical impedance spectroscopy (EIS), and 4) hybrid pulse power characterization (HPPC). Detailed procedures of each technique are described elsewhere.[36] During life cycle tests, cells were stopped periodically (for every 1 or 2 months between cycling tests) for characterization using the procedures described above. For each of the cells tested, the cell capacity measured at a C/20 rate till 100% DOD (or 0% state of discharge (SOD)) during characterization was used for the subsequent modeling work. Such a slow charging-discharging is performed for cell capacity measurement since it avoids any capacity inaccessibility due to impedance rise as a result fast charging. The capacity loss was normalized with its initial cell capacity. Commensurate with the model to be described, the cell cycling regime may be viewed as substantially full charge and discharge at low rates of operation, consistent with electric vehicle applications.

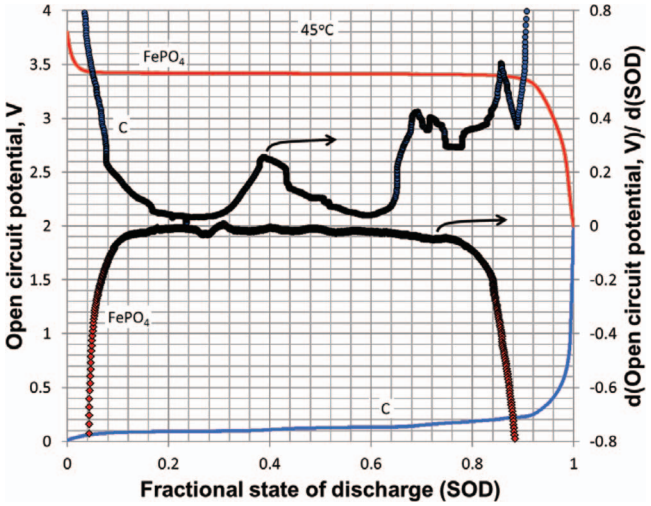

Figure 2. The solid curves are potential vs. state of discharge (SOD) curves for the graphite-$LiFePO_4$ cell (left ordinate). The curves comprised of symbols represent dV/d(SOD) against SOD for the individual electrodes (right ordinate). We find that the negative electrode dV/d(SOD) curve shows peaks for the graphite staging, and that the dV/d(SOC) curve for $FePO_4$ maintains a fairly constant value for a large SOD range (0.1 to 0.8 SOD).

Experimental Results

With a reference electrode arrangement[35] we could generate potential vs. state of discharge (SOD) curves for individual electrodes of a commercial C-LFP battery as shown in Fig. 2. We find that the $FePO_4$ electrode voltage is fairly constant for the entire SOD range, and the negative carbon electrode undergoes staging (i.e., phase transformations[38]) upon lithiation or delithiation. In Fig. 2, we plot the differential voltage [d(Voltage, V) /d(State of discharge (SOD)] against SOD for individual electrodes. We find that the negative electrode dV/d(SOD) curve shows peaks for the graphite staging; at the same time, the dV/d(SOD) curve for the $FePO_4$ electrode is fairly constant, with little variation.

With the experimental setting as described above, we could monitor the capacity fading of the batteries with cycling (90% depth of discharge and C/2 rate as noted above). The formation cycles were done prior to the cycling discussed here (manufactures normally deliver cells to end users that have already been cycled one or more times). We designate the first cycle of our testing to be cycle number 2. Fig. 3 shows the measured voltage (V) against cell capacity (Ah)

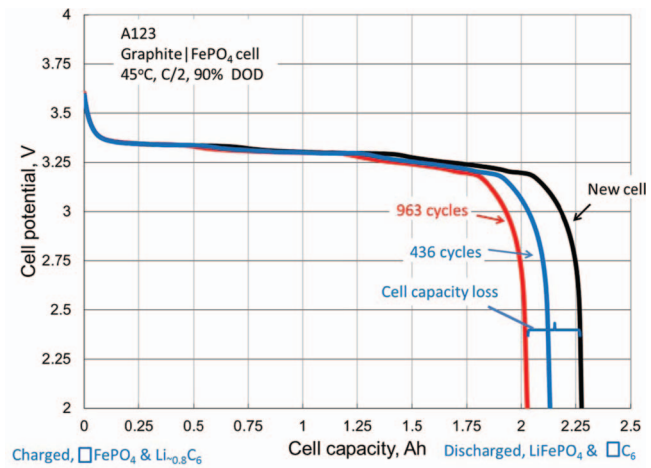

Figure 3. Plots of the measured voltage against the capacity for graphite-$LiFePO_4$ cell at 45°C at cycle numbers 2, 436, and 963.

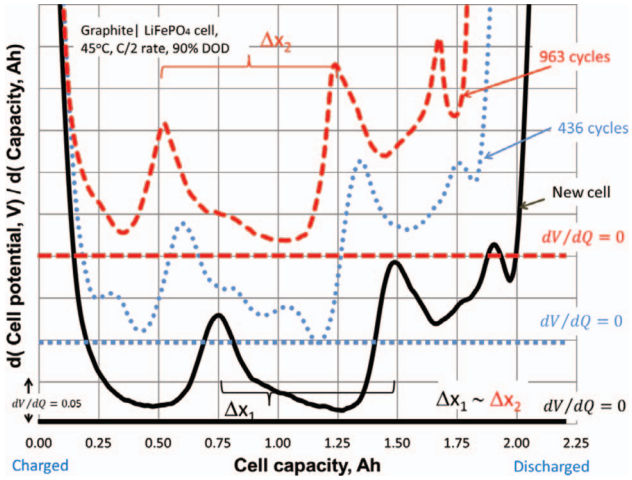

Figure 4. Plots of experimentally obtained differential voltages of the graphite-$LiFePO_4$ cell against the cell capacity (Ah) for at 45°C at cycle numbers 2, 436, and 963.

curves for C-LFP battery at 45°C at cycle numbers 2, 436, and 963. We find that as we cycle the battery, the discharge voltage is reached sooner, representing capacity loss. We calculate the differential voltage i.e. d(Voltage, V) /d(Capacity, Ah) for the full cell after different cycles and plot them against cell capacity (Ah) in Fig. 4. Since, there are no peaks in the differential voltage curves of the $FePO_4$ electrodes, as discussed previously, the significant peaks observed in the Fig. 4 correspond to the graphite staging in the full cell. The distance between two predominant peaks represents the amount of lithium that can be stored in the graphite electrode for a particular stage. The differential voltage curves in Fig. 4 are for the same cell cycled at cycle 2, 436, and 963. To make these curves more distinct, we shift the x axis up along the y-axis by 0.1 units for differential voltage curve after 436 cycles and by 0.2 units for differential voltage curve after 963 cycles. We find that the distance between the peaks in all three cases remains the same, and all of the curves shift to the left on cycling, with the capacity of the cells decreasing. Since, the distance between the peaks remain the same, the amount of active carbon sites to store the active lithium is substantially constant upon cycling. Thus, the shift of the differential voltage curves to left is consistent with the capacity loss being due to loss of active lithium from the system, and the evidence is compelling. To summarize, the measured differential voltage curves indicate that the capacity loss in these experiments is due to lithium loss in SEI formation, and most of the carbon is substantially unchanged and available for lithiation.

Mathematical Model

As described in the Theoretical Background section previously, we assume the capacity loss in a battery is solely caused by irreversible lithium loss on the negative electrode surface and that the negative and positive electrodes remain otherwise fully functional. For the substantially full charge and discharge at low rates of current (consistent with electric vehicle applications) and the C-LFP system, these assumptions are valid.

Due to complex nature of the problem—to establish a battery life model—we employ three widely accepted and established sub-models to formulate the life model:

1. Diffusion induced stresses (DIS): established diffusion and stress/strain equations
2. Crack growth: well-known Paris Law of mechanical fatigue based on empirical observations and theoretical justifications
3. SEI thickness growth: Based on past research employing a thickness to time to the 1/2 power observation.

In solid mechanics it is widely observed and discussed that a material undergoing cyclic loading is likely to experience fatigue and fracture. Electrode particles on lithiation and delithiation experience diffusion induces stresses (DISs). Through experimental observation and mathematical modeling the nature of DISs in lithium insertion electrodes are well established now (See Ref. 18–27). Crack growth upon cyclic stress is widely observed and discussed in the field of solid mechanics. These facts lead us to use Paris' law for crack growth on the electrode particles. Paris' law is a commonly used tool to model crack growth, leading to fatigue failure. Paris' law is based on empirical observations and theoretical justifications (see Ref. 38–45). Also, different studies about the calendar life of lithium ion batteries suggest that SEI thickness grows with time and is proportional to square root of time (See Ref. 4 and 12). The total loss of capacity can be understood by combining these three physical processes, and that is the purpose of this paper.

The total lithium loss during cycling can be divided in the following four scenarios.

i. Lithium loss on SEI formation in first cycle. This is related to the SEI formation over the entire surface of the active particles of the negative electrode.
ii. Lithium loss due to SEI formation on newly formed surfaces due to crack propagation during subsequent cycles.
iii. Lithium loss due to continued SEI thickness growth of the SEI formed during the first (i.e., the formation) cycle.
iv. Lithium loss due to continued SEI thickness growth on the newly formed surfaces due to crack propagation.

The first cycle capacity loss is related to the initial particle surface area. The total capacity loss after initial SEI formation cycles, i.e., after the first cycle, can be calculated using the respective mechanism (ii), (iii) and (iv) as

$$\frac{dQ}{dN} = \frac{dQ}{dN}_{SEI\ formation\ due\ to\ crack\ propagation} + \frac{dQ}{dN}_{SEI\ thickness\ growth\ on\ initial\ surface} + \frac{dQ}{dN}_{SEI\ thickness\ growth\ on\ cracked\ surface} \quad [1]$$

respectively.

Loss of lithium due to SEI formation on newly formed surfaces due to crack propagation.— As is often done, we shall assume that the diffusion in the spherical particle for galvanostatic charging condition can be described with the Fick's law of diffusion. The diffusion equation for transport inside the electrode particle can be written as

$$\frac{\partial C}{\partial t} = \frac{\mathcal{D}_\alpha}{r^2}\frac{\partial}{\partial r}\left(r^2\frac{\partial C}{\partial r}\right) \quad [2]$$

with initial and boundary conditions:

$$\begin{aligned} &C(r,0) = C_0, && for\ 0 \le r \le R \\ &D\frac{\partial C(r,t)}{\partial r}\bigg|_{r=R} = \frac{i}{F}, && for\ t \ge 0 \\ &C(0,t) = finite, && for\ t \ge 0 \end{aligned} \quad [2a]$$

Here '*i*' is the current over particle surface. The solution for galvanostatic condition is well-known[39]:[d]

$$c(x,\tau) = c_0 + \frac{iR}{FD}\left[3\tau + \frac{1}{2}x^2 - \frac{3}{10} - \frac{2}{x}\sum_{n=1}^{\infty}\left(\frac{\sin(\lambda_n x)}{\lambda_n^2 \sin(\lambda_n)}e^{-\lambda_n^2\tau}\right)\right] \quad [3]$$

[d]The concentration $C(r, t)$ must be greater than zero and cannot exceed the concentration of available sites for the solute in the case of insertion electrodes, and this will place limits on the admissible values of the product *It*.

where $x = r/R, \tau = tD/R^2$, positive current densities i over the particle surface denote charge, and $\lambda_n (n = 1, 2, 3, \ldots)$ are the positive roots of $\tan(\lambda_n) = \lambda_n$. For a thin film electrode with a specific surface area a_s, thickness L, and geometric area A and the cell current I_{cell}, the current density over a particle surface i can be calculated as

$$i = \frac{I_{cell}}{a_s\,(AL)_{PE}} \quad [4]$$

The specific surface a_s of the porous electrode is related to the radius R of the active spherical particles and overall their contribution to the solid phase porosity ε_{1a}, $a_s = 3\varepsilon_{1a}/R$. Hence,

$$i = \frac{I_{cell} R}{3\varepsilon_{1a}\,(AL)_{PE}} \quad [4a]$$

Cheng and Verbrugge[39] showed the maximum stress in a cell is at the surface of the electrode in the tangential direction at the start of discharge. The magnitude of this stress is described as

$$\sigma_\theta = \frac{1}{3}\frac{E\Omega}{(1-\nu)}\left(\frac{iR}{FD}\right)\left[\frac{1}{5}(1-2x^2) + 2\sum_{n=1}^{\infty}\frac{e^{-\lambda_n^2\tau}}{\lambda_n \sin(\lambda_n)} \times \left(\frac{\sin(\lambda_n x)}{\lambda_n x} - \frac{\sin(\lambda_n x) - (\lambda_n x)\cos(\lambda_n x)}{\lambda_n^3 x^3}\right)\right] \quad [5]$$

where E is the Young's modulus and ν is the Poisson's ratio of the electrode material, and Ω is the partial molar volume of the solute.

For our low rate, deep discharge (electric vehicle) investigation, we are interested in longer times, consistent with the fact that our charge and discharge cycles are much longer than R^2/D, the characteristic time for solid state diffusion of lithium within the host negative electrode. Hence, the exponential terms in the stress equations tend to zero, and summations can be neglected. Because the magnitude of the tangential stress σ_θ increases monotonically to an asymptote and is largest at the particle surface, we shall refer to the long-time asymptotic value of the surface tangential stress as $\sigma_{\theta,\max}$. Second, we shall restrict our attention to cracks formed and growing at the particle surface. Because the particle is taken to be isolated, and we do not account for surface mechanics (e.g., surface tension) associated with nm size particles[29] the radial component of the stress at the surface is zero, and the aforementioned maximum tangential stress at the surface corresponds to

$$\sigma_{\theta,max} = -\frac{1}{15}\frac{E\Omega}{(1-\nu)}\left(\frac{iR}{FD}\right) = -\frac{1}{45}\frac{E\Omega}{(1-\nu)}\left(\frac{R^2}{FD}\right)\frac{I_{cell}}{\varepsilon_{1a}\,(AL)_{PE}} \quad [6]$$

In terms of stress over a cycle, the surface undergoes tensile stress during the majority of the discharge process in accordance with Eq. 6. During charge, there is a very slight compression at the surface due to DIS. We employ the Paris' Law formulation to represent a surface crack of length a growing with each charge-discharge cycle N,[40–42]

$$\frac{da}{dN} = k\Delta K_I^m \quad [7]$$

where k and m are taken to be constants, and the difference in the mode I stress intensity factor K_I between the fully loaded state, corresponding to the steady-state constant current discharge, and the charge state is given by

$$\Delta K_I = \sigma_{\theta,max} b\sqrt{\pi a} \quad [8]$$

Hence, we shall only employ the discharge (tensile) state for crack propagation. For the small surface cracks we investigate $a \ll R$, and the constant $b = 1.12$.[43] Substituting Eqs. 6 and 8 into Eq. 7, we obtain

$$\frac{da}{dN} = k[\sigma_{\theta,max} b\sqrt{\pi a}]^m \quad [9]$$

$$\frac{da}{dN} = k\left[-\frac{1}{45}\frac{E\Omega}{(1-\nu)}\left(\frac{R^2}{FD}\right)\frac{I_{cell}}{\varepsilon_{1a}\,(AL)_{PE}} b\sqrt{\pi a}\right]^m \quad [10]$$

$$a_0\frac{d\tilde{a}}{dN} = k[\sigma_{\theta,max} b\sqrt{\pi a}]^m = k[\sigma_{\theta,max} b\sqrt{\pi a_0}]^m \tilde{a}^{m/2} \quad [11]$$

$$\frac{d\tilde{a}}{d\tilde{N}} = \tilde{a}^{m/2} \quad [12]$$

Here, for simplicity we define

$$\tilde{N} = k[\sigma_{\theta,max} b\sqrt{\pi}]^m a_0^{\left(\frac{m-2}{2}\right)} N \quad \text{and} \quad \tilde{a} = a/a_0$$

Integrating Eq. 12, we obtain

$$\int_1^{\tilde{a}} \frac{d\tilde{a}}{\tilde{a}^{m/2}} = \int_0^{\tilde{N}} d\tilde{N}$$

$$\tilde{a} = \left(1 + \frac{2-m}{2}\tilde{N}\right)^{\frac{2}{2-m}}$$

$$\tilde{a} = \left(1 + \frac{2-m}{2}k[\sigma_{\theta,max} b\sqrt{\pi}]^m a_0^{\left(\frac{m-2}{2}\right)} N\right)^{\frac{2}{2-m}} \quad [13]$$

Eq. 13 relates the crack depth with the number of cycles. As a crack grows during discharge, the newly exposed surface of area is $2l_{cr}(da)$, where l_{cr} is the length of the crack.

We take the number of cracks and the length of each crack to be the same throughout this particle life; that is, the cracks are all taken to be identical and grow in depth into the particle during each discharge half cycle. While we have no direct evidence for this for lithiated graphites, References 44 depict this type of behavior for lithiation of high capacity metals (i.e., initially established cracks provide strain relief upon discharge, and new cracks do not form to a significant extent). Hence, ρ_{cr} is defined as the surface crack density; i.e., the number of cracks per unit area of particle surface. We shall treat the surface density of the cracks as a constant, and it is given by the initial number of cracks over the particle surface, $N_{cr} = 4\pi R^2 \rho_{cr}$. The total area associated with cracks is given by $A_{cr} = 8\pi R^2 \rho_{cr} a l_{cr}$. We can express the change in the total area associated with cracks for each discharge cycle as

$$\frac{dA_{cr}}{dN} = \frac{dA_{cr}}{da}\frac{da}{dN} = 8\pi R^2 l_{cr}\rho_{cr} k[\sigma_{\theta,max} b\sqrt{\pi a_0}]^m \tilde{a}^{m/2} \quad [14]$$

We assume the newly exposed surface is covered by SEI over the next charge cycle, as described earlier about the formation of Li_2CO_3. SEI forms on the newly cracked surface as soon as it is exposed to the electrolyte, forming a layer of thickness L_{SEI}^0.

$$\frac{dQ}{dN}_{SEI\ formation\ due\ to\ crack\ propagation} = -\frac{n_{SEI} L_{SEI}^0 \rho_{SEI} F}{M_{SEI}}\frac{dA_{cr}}{dN}$$

$$= -\frac{n_{SEI} F L_{SEI}^0 \rho_{SEI} 8\pi R^2 l_{cr}\rho_{cr}}{M_{SEI}}[\sigma_{\theta,max} b\sqrt{\pi a_0}]^m k\tilde{a}^{m/2} \quad [15]$$

where n_{SEI} is the number of lithium atoms lost per SEI molecule formed, ρ_{SEI} is the density of the SEI film formed, M_{SEI} is the molecular weight of the compound constituting SEI. Combining Eqs. 13 and 15, we obtain

$$\frac{dQ}{dN}_{SEI\ formation\ due\ to\ crack\ propagation} = -\frac{n_{SEI} F L_{SEI}^0 \rho_{SEI} 8\pi R^2 l_{cr}\rho_{cr}}{M_{SEI}}[\sigma_{\theta,max} b\sqrt{\pi a_0}]^m k \times \left(1 + \frac{2-m}{2}k[\sigma_{\theta,max} b\sqrt{\pi}]^m a_0^{\left(\frac{m-2}{2}\right)} N\right)^{\frac{m}{2-m}} \quad [16]$$

Lithium loss due to increase in the thickness L_{SEI} of the initial SEI layer.— Along with crack propagation, an increase in the thickness of the existing SEI upon cycling also contributes to the lithium loss from the cell. The increase in SEI thickness has been observed by several groups by increase in the resistance of the cell.[14] Most of the calendar life experiments and models assume that the thickness is time dependent and is proportional to square root of time.[6] Since, the functional form of SEI growth during cycling is unknown, we assume SEI growth with the following equation

$$L_{SEI} = K_{th} N^{1/2} \quad [17]$$

Here, K_{th} is a constant and is temperature dependent. Note that a very simple model formulation would be to assume that the SEI grows immediately to its final thickness at the end of each discharge cycle upon which the crack surface was first exposed. Eq. 17 provides an enhancement wherein the SEI thickness continues to grow upon subsequent cycling.

Lithium loss due to increase in the thickness L_{SEI} of the initial SEI layer.— The first cycle leads to the initial SEI formation (often referred to as the formation cycle). On the first cycle, we assume that all of the surface area is covered with SEI of thickness L^0_{SEI}. From the second cycle onwards, the SEI formed during the first cycle grows in thickness. The initial surface area of the spherical particle after the formation cycle is the surface area of sphere with pre-existing cracks

$$\begin{aligned} A_{initial} &= \textit{spherical surface area} \\ &\quad + \textit{area associated with preexisting cracks} \\ &\quad \textit{on the surface} \\ A_{initial} &= 4\pi \left(R + L^0_{SEI}\right)^2 + 8\pi R^2 l_{cr} \rho_{cr} a_0 \end{aligned}$$

For commercial batteries, the particle radius is about 5 microns. In Parameters and Assumption Section, we find that the L^0_{SEI} is in few nanometers range; hence, $L^0_{SEI} \ll R$. Thus, we approximate $R + L^0_{SEI} \sim R$ and obtain the following equation for initial surface area of the spherical particle.

$$A_{initial} = 4\pi R^2 \left(1 + 2 l_{cr} \rho_{cr} a_0\right)$$

Hence, the rate of capacity loss upon subsequent cycling due to continued growth in thickness of SEI that was formed in the first cycle is given by

$$\begin{aligned} &\frac{dQ}{dN}_{SEI\ thickness\ growth\ on\ initial\ surface} \\ &= -\frac{n_{SEI} F \rho_{SEI}}{M_{SEI}} A_{initial} \frac{dL_{SEI}}{dN} \\ &= -\frac{n_{SEI} F \rho_{SEI}}{M_{SEI}} 4\pi R^2 \left(1 + 2 l_{cr} \rho_{cr} a_0\right) \frac{dL_{SEI}}{dN} \end{aligned} \quad [18]$$

Differentiating Eq. 17 with respect to number of cycles N, we obtain

$$\frac{dL_{SEI}}{dN} = \frac{1}{2} K_{th} N^{-1/2} \quad [19]$$

which, when combined with Eq. 18, yields

$$\begin{aligned} &\frac{dQ}{dN}_{SEI\ thickness\ growth\ on\ initial\ surface} \\ &= -\frac{n_{SEI} F \rho_{SEI}}{M_{SEI}} 4\pi R^2 \left(1 + 2 l_{cr} \rho_{cr} a_0\right) \frac{1}{2} K_{th} N^{-1/2} \end{aligned} \quad [20]$$

Loss of lithium due to growth of SEI thickness in the cracked area.— There is an incremental increase in the new surface area each cycle. As soon as a new area is exposed to electrolyte SEI is formed on this area upon subsequent lithiation. The SEI formed in this cracked area grows in thickness in the subsequent cycles. For cycle N, the area of crack opened on first cycle would have gone through *N-1* cycles, thus thickness growth related to *N-1* cycles would occur on that area. Similarly, on cycle N, the crack area opened on second cycle would undergo *N-2* cycles hence a thickness growth related to *N-2* cycles. Capacity loss in the cracked area on cycle N can be mathematically written as;

$$\begin{aligned} &\frac{dQ}{dN}_{SEI\ thickness\ growth\ on\ cracked\ surface} \\ &= -\left[\frac{n_{SEI} F \rho_{SEI}}{M_{SEI}} \left(\frac{dA_{cr}}{dN}\right)_1 \left(\frac{dL_{SEI}}{dN}\right)_{N-1} \right. \\ &\quad + \frac{n_{SEI} F \rho_{SEI}}{M_{SEI}} \left(\frac{dA_{cr}}{dN}\right)_2 \left(\frac{dL_{SEI}}{dN}\right)_{N-2} + \cdots \\ &\quad \left. + \frac{n_{SEI} F \rho_{SEI}}{M_{SEI}} \left(\frac{dA_{cr}}{dN}\right)_{N-1} \left(\frac{dL_{SEI}}{dN}\right)_1 \right] \end{aligned}$$

$$\begin{aligned} &\frac{dQ}{dN}_{SEI\ thickness\ growth\ on\ cracked\ surface} \\ &= -\frac{n_{SEI} F \rho_{SEI}}{M_{SEI}} \sum_{i=1}^{N-1} \left(\frac{dA_{cr}}{dN}\right)_i \left(\frac{dL_{SEI}}{dN}\right)_{N-i} \end{aligned} \quad [21]$$

(As mentioned previously, our experiments begin with cycle $N = 2$.) The capacity loss in the cracked area due to SEI growth in the subsequent cycles is given as

$$\begin{aligned} &\frac{dQ}{dN}_{SEI\ thickness\ growth\ on\ cracked\ surface} \\ &= -\frac{n_{SEI} F \rho_{SEI}}{M_{SEI}} \sum_{i=1}^{N-1} 8\pi R^2 l_{cr} \rho_{cr} k [\sigma_{\theta,max} b \sqrt{\pi a_0}]^m \\ &\quad \times \left(1 + \frac{2-m}{2} k [\sigma_{\theta,max} b \sqrt{\pi}]^m a_0^{\left(\frac{m-2}{2}\right)} (N-i)\right)^{\frac{m}{2-m}} \\ &\quad \times \frac{1}{2} K_{th} (N-i)^{-1/2} \end{aligned} \quad [22]$$

Total lithium loss after formation cycles.— After the formation cycle, the rate of capacity loss in the subsequent cycles is given by Eq. 1

$$\begin{aligned} \frac{dQ}{dN} &= \frac{dQ}{dN}_{SEI\ formation\ due\ to\ crack\ propagation} \\ &\quad + \frac{dQ}{dN}_{SEI\ thickness\ growth\ on\ initial\ surface} \\ &\quad + \frac{dQ}{dN}_{SEI\ thickness\ growth\ on\ cracked\ surface} \end{aligned}$$

Thus, combining Eqs. 16, 20 and 21, we get,

$$\begin{aligned} \frac{dQ}{dN} &= -\frac{n_{SEI} F L^0_{SEI} \rho_{SEI} 8\pi R^2 l_{cr} \rho_{cr}}{M_{SEI}} [\sigma_{\theta,max} b \sqrt{\pi a_0}]^m k \\ &\quad \times \left(1 + \frac{2-m}{2} k [\sigma_{\theta,max} b \sqrt{\pi}]^m a_0^{\left(\frac{m-2}{2}\right)} N\right)^{\frac{m}{2-m}} \\ &\quad - 4\pi R^2 \frac{n_{SEI} F \rho_{SEI}}{M_{SEI}} \left(1 + 2 l_{cr} \rho_{cr} a_0\right) \frac{1}{2} K_{th} (N)^{-1/2} \\ &\quad - \frac{n_{SEI} F \rho_{SEI}}{M_{SEI}} \sum_{i=1}^{N-1} 8\pi R^2 l_{cr} \rho_{cr} k [\sigma_{\theta,max} b \sqrt{\pi a_0}]^m \\ &\quad \times \left(1 + \frac{2-m}{2} k [\sigma_{\theta,max} b \sqrt{\pi}]^m a_0^{\left(\frac{m-2}{2}\right)} (N-i)\right)^{\frac{m}{2-m}} \\ &\quad \times \frac{1}{2} K_{th} (N-i)^{-1/2} \end{aligned} \quad [23]$$

We obtain the fractional capacity loss by dividing the equation by Q_0, the capacity of the electrode immediately after the formation cycle (the capacity of the cell for the second cycle).

The efficiency of the formation cycle η_1 and the capacity of the cell before the formation cycle $Q_0^{initial}$ are related to the capacity Q_0:

$$Q_0 = \eta_1 Q_0^{initial} \quad [24]$$

In a typical lithium ion battery, the anode always has excess capacity relative to the cathode. The cell capacity is, therefore, limited by the cathode capacity. The initial capacity is

$$Q_0^{initial} = initial\ capacity = \frac{(specific\ capacity\ of\ graphite\ anode, Ah/g)\left(\frac{4}{3}\pi R^3 \rho_{graphite}\right)}{q_r} \quad [25]$$

where

$$q_r = \frac{Anode\ capacity,\ Ah}{Cathode\ capacity,\ Ah}$$

In a conventional lithium ion cell employing a substantially graphitic negative electrode, the negative's capacity is about 10% greater than that of the positive in order to avoid lithium plating on overcharge of the negative. For such a cell, $q_r = 1.1$. To simplify notation, we define

$$A = l_{cr}\rho_{cr}[\sigma_{\theta,max} b\sqrt{\pi a_0}]^m k,$$

$$B = \frac{n_{SEI} F \rho_{SEI} 4\pi R^2}{M_{SEI} Q_0}, \quad \text{and} \quad C = -\frac{2-m}{2} k[\sigma_{\theta,max} b\sqrt{\pi}]^m a_0^{\left(\frac{m-2}{2}\right)}$$

Here the parameters A, B, and C are all positive. Note that a typical value of m in fracture mechanics is between 2 and 5[45–47]

$$\frac{d\breve{Q}}{dN} = -2BAL_{SEI}^0 (1-CN)^{\frac{m}{2-m}} - B(1+2l_{cr}\rho_{cr}a_0)\frac{1}{2}K_{th}(N)^{-1/2} - 2BA\sum_{i=1}^{N-1}(1-C(N-i))^{\frac{m}{2-m}}\frac{1}{2}K_{th}(N-i)^{-1/2} \quad [26]$$

Integrating, we obtain the fractional cell capacity $\breve{Q}$

$$\breve{Q} - 1 = +\frac{2-m}{C}BAL_{SEI}^0\left((1-CN)^{\frac{2}{2-m}} - (1-C)^{\frac{2}{2-m}}\right) - BK_{th}(1+2l_{cr}\rho_{cr}a_0)((N)^{1/2}-1) - BAK_{th}\int_1^N \sum_{i=2}^{N-1}(1-C(N-i))^{\frac{-m}{m-2}}(N-i)^{-1/2}dN \quad [27]$$

We numerically integrate this equation to get the fractional capacity as a function of cycle number. Note that the solution is analytic if we assume the SEI grows immediately to its final thickness at the end of each discharge cycle upon which the crack surface was first exposed i.e. SEI thickness does not grow once it is formed

$$\breve{Q} = 1 + \frac{2-m}{C}BAL_{SEI}^0\left((1-CN)^{\frac{2}{2-m}} - (1-C)^{\frac{2}{2-m}}\right) \quad [28]$$

First Cycle SEI Formation Lithium Loss and Estimation of L_{SEI}^0

The capacity lost in initial SEI formation around a particle is

$$Q_{lost} = A_{initial}\frac{n_{SEI}FL_{SEI}^0\rho_{SEI}}{M_{SEI}} \quad [29]$$

On the first cycle we assume that all the surface area of surface and pre-existing cracks at the surface would be covered with SEI of thickness L_{SEI}^0

$$A_{initial} = 4\pi R^2 + 8\pi R^2 l_{cr}\rho_{cr}a_0 = 4\pi R^2(1+2l_{cr}\rho_{cr}a_0) \quad [30]$$

Hence,

$$Q_{lost} = A_{initial}\frac{n_{SEI}FL_{SEI}^0\rho_{SEI}}{M_{SEI}} \quad [31]$$

$$Q_{lost} = 4\pi R^2(1+2l_{cr}\rho_{cr}a_0)\frac{n_{SEI}FL_{SEI}^0\rho_{SEI}}{M_{SEI}} \quad [32]$$

To simplify notation, we employ

$$B^0 = \frac{n_{SEI}F\rho_{SEI}4\pi R^2}{M_{SEI}Q_0^{initial}}$$

Thus Eq. 32 becomes,

$$\frac{Q_{lost}^{formation\ cycle}}{Q_0^{initial}} = (1+2l_{cr}\rho_{cr}a_0)L_{SEI}^0 B^0 \quad [33]$$

Hence, if the formation cycle efficiency is known, the initial SEI thickness L_{SEI}^0 can be calculated as follows

$$L_{SEI}^0 = \frac{\frac{Q_{lost}^{formation\ cycle}}{Q_0^{initial}}}{(1+2l_{cr}\rho_{cr}a_0)B^0} = \frac{1-\eta_1}{(1+2l_{cr}\rho_{cr}a_0)B^0} \quad [34]$$

Parameters and Assumptions

We assume the initial crack depth and length to be $a_0 = l_{cr} = 2\,nm$, and that the initial crack density ρ_{cr} corresponds to 8×10^8 cracks on the surface of a spherical electrode particle of 5 micrometer radius. The particle size for the calculations is consistent with commercial electrodes.[37] The solid phase porosity ε_{1a} of the electrode film is taken to be 65%.[37] The value of Paris' law constant m is assumed to be 2.5 which is consistent with the typical value for ductile but hard materials.[41] The Young's modulus of graphite is taken to be $33\times10^9 Nm^{-2}$.[48] The diffusion coefficient of lithium ions within the lithiated graphite is taken to be $10^{-14} m^2/sec$.[49]

Crack propagation as well as SEI growth rate are thermally activated processes. Hence, we assume Paris' law constant k as well as thickness growth constant K_{th} follow an Arrhenius dependence

$$k = k_0 e^{(-E_{a1}/RT)} \text{ and } K_{th} = K_{th}^0 e^{(-E_{a2}/RT)} \quad [35]$$

We treat k_0 and K_{th}^0 as fitting parameters in the model. We find that the activation energy for crack propagation is $19.37\,kcal\,mol^{-1}$ and that for the SEI thickness growth is $9.44\,kcal\,mol^{-1}$. As discussed earlier, we assume that all of the SEI formed upon crack propagation consists of Li_2CO_3, thus there are two moles lithium lost for every mole of Li_2CO_3 formed during cycling ($n = 2$). We take the molecular weight of Li_2CO_3 as the molecular weight of the SEI. The formation cycle efficiency η_1 is assumed to be 90% i.e. 10% loss of capacity in the formation cycle. Using these parameters in the Eq. 34, we calculate the initial SEI thickness to be $L_{SEI}^0 \sim 3.5\,nm$. In these calculations this SEI thickness grows gradually from 3.5nm upto 15 nm in the subsequent 2000 cycles, depending upon the operating temperature conditions. Higher operating temperature leads to thicker SEI for same duration of operation. For fitting the experimental data, the different values of k and K_{th} are chosen with the same m, ρ_{cr}, l_{cr} and a_0 values. These values are used to calculate the k_0, K_{th}^0, E_{a1}, and E_{a2} using the Arrhenius dependence. With the present parameters k_0 was found to be 1.6×10^{-9} and K_{th}^0 is found to be 2.75×10^{-4}. Appendix A at the end of paper explains in details about the how different parameters are obtained.

Results and Discussion

With the assumptions stated above, we plot the capacity fading of the cell as a function of cycles for different temperatures using Eq. 27. For calculating this, we assumed the capacity of cells after formation cycles (Q_0) to be 2.25 Ah. In Fig. 5, the dots represent the experimental data of the capacity of the cell and the solid lines represent the model

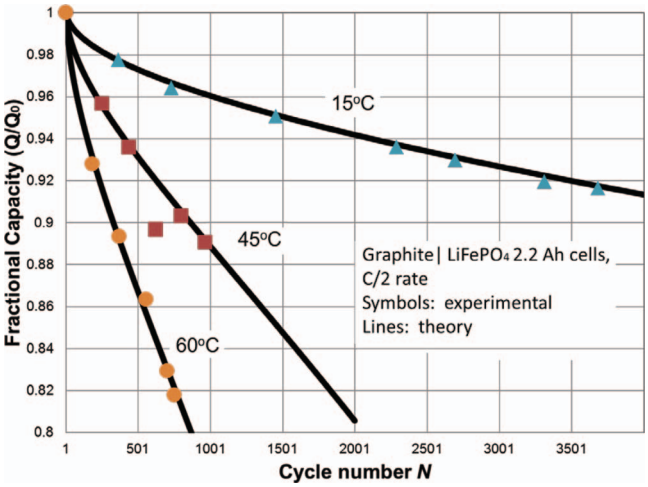

Figure 5. A plot of the capacity fading of the cell as a function of number of cycles for different temperatures. The dots represent the experimental data of the capacity of the cell and the solid lines represent the calculated capacity using the model.

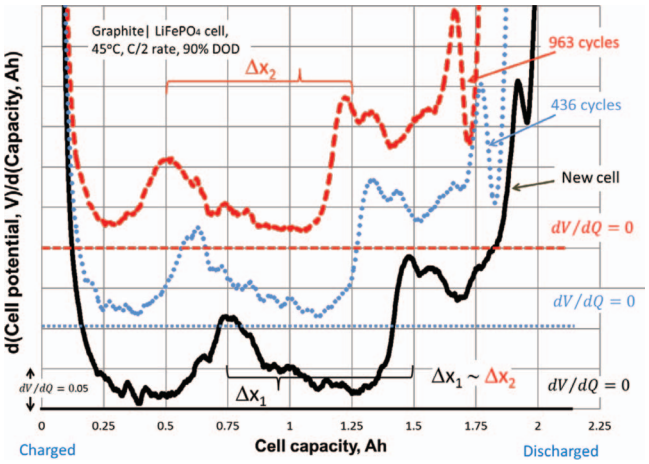

Figure 7. Plots of differential voltages (dV/dQ) against capacity (Ah) for different cycle numbers obtained using the proposed model for different cycle numbers.

calculation. We find that the model is in good agreement with the experimental data, suggesting that the basic theory is able to capture the observed phenomena using reasonable parameter values. To quantify the deviation of the model from the experiments, we calculated the average of square of deviation of calculated fractional capacities from the experimental fractional capacities normalized with the experimental fractional capacity i.e. $error = (\frac{\breve{Q}_{experimental} - \breve{Q}_{calculated}}{\breve{Q}_{experimental}})^2$. These errors are found to be 3.23×10^{-6}, 9.45×10^{-5} and 4.24×10^{-5} for cells cycled at 30, 45 and 60°C respectively. These errors are quite small and reflect a high correlation between the model and the cycled cells that were cycled to failure (cf. Fig. 5).

To further test the model, we generate the individual electrode voltage vs. capacity curves (Fig. 6) at various cycles. We use the SOD vs. potential charts of the individual electrodes as a lookup table to generate these curves. The curves in Fig. 6 match well with the experimental curves in Fig. 3. Next, we calculate the differential voltage (dV/dQ) curves using the voltage curves of Fig. 6, allowing us to generate dV/dQ vs. Q (Q in Ah) for different cycle numbers depicted in Fig. 7. To make these curves more distinct, we shift the x axis up along the y-axis by 0.1 units for differential voltage curve after 436 cycles and by 0.2 units for differential voltage curve after 963 cycles. We compare these plots with the experimental plots in Fig. 4 and find that they are in good agreement. Again, we observe that the distance between the differential voltage (dV/dQ) peaks remain the same as we cycle the battery. This is consistent with our assumption that lithium loss due to incremental SEI formation on the negative electrode, including the influence of crack propagation and subsequent passivation, is the main mechanism of capacity fading, and there is no loss of active host (graphite) materials.

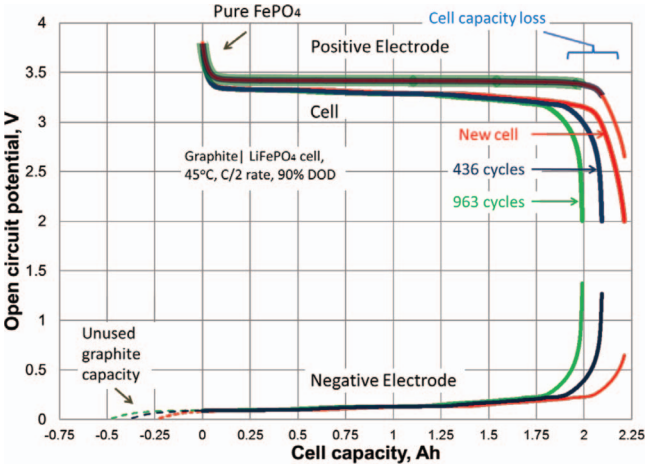

Figure 6. Plots of voltage (V) vs. capacity (Ah) at different number of cycles for the data calculated using the model. The lowermost three curves represent the negative electrode potential at different cycles, and the uppermost curves, which overlay one another for most of the voltage range, depict the positive electrode potential. The middle three curves correspond to the cell potential.

Knowing the SOD of the individual electrodes, we can generate the full cell voltage plots using the individual electrode voltages previously shown in Fig. 6. We see that as we cycle the cell, initially there is an increase in the voltage of $FePO_4$ electrode (against a lithium reference electrode) at the end of discharge, since it cannot be completely lithiated, as lithium has been lost to SEI formation on the negative electrode. Once enough lithium is lost, the positive electrode maintains a potential on the two-phase constant-voltage plateau (near 3.4 V vs. lithium), and variations in cell voltage toward the end of discharge are due to the rise in potential of the graphitic electrode relative to a lithium reference.

As noted previously, cells often employ about 10% negative capacity than that of the positive. Thus there is always some unused capacity of graphite at the end of charging in the first cycle. As the capacity fades on cycling, the graphite electrode cannot be completely lithiated, and the capacity utilization of the graphite is reduced when the only capacity loss mechanism is lithium consumption. As plotted, the graphite voltage curve shifts to left on cycling, corresponding to the shift in peaks in the differential voltage curves of the full cell (Fig. 7).

Conclusions

1. We have developed the first model that couples electrochemistry, chemical degradation (including SEI formation), and fracture mechanics so as to clarify life performance of a lithium ion cell. We examine a graphite-$LiFePO_4$ cell cycled over a broad temperature range and at relatively low rates of charge and discharge, consistent with electric vehicle applications.
2. We find good agreement between the modeling results and experimental observations. Specifically:
   a. The voltage vs. capacity curves and differential voltage vs. capacity curves generated with the model are found to be in good agreement with the experimental data when reasonable parameter values are employed.

b. Experimentally and theoretically, we are able to deconvolute the cell voltage curves into individual electrode voltages and clarify the state of the individual electrodes upon electrochemical cycling.
c. The model captures the capacity versus cycle number relationship over a broad temperature range.

Acknowledgments

Rutooj Deshpande thank General Motors for a Summer Internship during which the main part of this research was carried out. The authors would also like to thank Dr. Yue Qi and Dr. Stephen Harris of GM R&D and Dr. Justin Purewal from HRL Laboratories for helpful discussions. Financial support from NSF (CMMI #1000726) and General Motors R&D Center is greatly acknowledged.

Appendix A: A Summary of Parameters Used in the Battery Cycle Life Model

DIS	Paris' Law	SEI Thickness Growth	1st Cycle Capacity Loss
D	m**		a_0*
E	k_0**	K_{th}^0 **	l_{cr}*
F	E_{a1} @	E_{a2} @	**L**
$\mathbf{I_{cell}}$			$\varepsilon_{1\alpha}$
L			η_1***
$\varepsilon_{\mathbf{1}\alpha}$			ρ_{cr}**

Parameters in **'bold'** are either material/electrode properties or operating conditions of the experiment.

Parameters followed by * are assumptions for the models.

Nano-cracks are observed on the particles of a new battery (see Ref. 24). Due to lack of experimental data about the dimensions of these cracks, we started with the assumptions for values of initial crack depth a_0 and crack length l_{cr} of the pre-existing cracks on the surface. To avoid further complication we started with the simplified assumption that all the pre-existing cracks have same dimensions. These assumptions are kept constant throughout the analysis.

On the other hand all the quantities followed by ** are found simply by fitting the following experimental observations.

1. The 1st cycled capacity loss in a battery is observed to be approximately 10% in well-made battery.
2. The capacity loss of a battery changes with cycling rate and temperature.

Parameters followed by *** correspond to direct measurement or observation.

Parameters followed by @ are calculated values after fitting the parameters to the experimental observations.

List of Symbols

A	geometric area of the electrode film (m^2)
a_s	specific surface area (m^{-1})
A	depth of a crack (m)
a_0	depth of a pre-existing crack (m)
A_{cr}	surface area in the cracks (m^2)
C(r, t)	solute concentration at radius r at time t (mol m^{-3})
C_0	initial solute concentration in the particle (mol m^{-3})
D	diffusion coefficient of the solute in solid phase (m^2 sec^{-1})
E	Young's modulus of the electrode material (N m^{-2})
E_{a1}	activation energy for crack propagation (kcal mol^{-1})
E_{a2}	activation energy for SEI thickness growth (kcal mol^{-1})
F	Faraday's constant (C)
I	current over electrode particle surface (A)
I_{cell}	cell current (A)
k, m	Paris' law parameters
K_I	stress intensity factor (N $m^{-3/2}$)
K_{th}	SEI thickness growth parameter
k_0	Arrhenius constant for Paris' Law parameter k
K_{th}^0	Arrhenius constant for thickness growth parameter K_{th}
L	thickness of electrode film (m)
l_{cr}	depth of a pre-existing crack (m)
L_{SEI}^0	initial SEI thickness (m)
L_{SEI}	SEI thickness (m)
M_{SEI}	molecular weight of compounds constituting SEI (gm mol^{-1})
N	number of charge-discharge cycles
N_{cr}	number of cracks over the particle surface
n_{SEI}	number of lithium atoms per SEI molecule formed
Q	capacity of the cell (Ah)
Q_0	capacity after formation cycle (Ah)
$Q_0^{initial}$	initial capacity before formation cycle (Ah)
q_r	ratio of initial anode capacity to initial cathode capacity
$\mathring{Q}$	fractional cell capacity
Q_{lost}	capacity lost in initial SEI formation around a particle (Ah)
R	radius of the spherical electrode particle (m)
r, θ, φ	spherical coordinates
T	time (sec)
X	dimensionless radius

Greek Symbols

$\varepsilon_{1\alpha}$	solid phase porosity of the electrode film
η_1	formation cycle efficiency
ρ_{SEI}	density of SEI films (gm m^{-3})
ρ_{cr}	number of cracks per unit area of the particle (m^{-2})
σ_θ	tangential stress (N m^{-2})
$\sigma_{\theta,max}$	maximum tangential stress (N m^{-2})
T	dimensionless time
Ω	partial molar volume of the solute (m^3 mol^{-1})

List of Parameters

A	geometric area of the graphite electrode film with 0.1 mA average current (m^2)	1.17×10^{-5} (m^2)
a_0	depth of a pre-existing crack (m)	2×10^{-9} (m)
D	diffusion coefficient of the solute in solid phase (m^2 sec^{-1})	10^{-14} $(m^2\ sec^{-1})$
E	Young's modulus of the electrode material (N m^{-2})	$3.3 * 10^{10}$ (N m^{-2})
E_{a1}	activation energy for crack propagation (kcal mol^{-1})	19.37 $kcal\ mol^{-1}$
E_{a2}	activation energy for SEI thickness growth (kcal mol^{-1})	9.44 $kcal\ mol^{-1}$
F	Faraday's constant (C)	96500 C
I_{cell}	cell current (A)	0.1 mA
k_0	Arrhenius constant for Paris' Law parameter k	1.6×10^{-9}
K_{th}^0	Arrhenius constant for thickness growth parameter K_{th}	2.75×10^{-4}
M	Paris' law parameter	2.5
L	thickness of electrode film (m)	38×10^{-6} (m)
l_{cr}	length of a pre-existing crack (m)	2×10^{-9} (m)
M_{SEI}	molecular weight of compounds constituting SEI (gm mol^{-1})	78.89 $(gm\ mol^{-1})$
q_r	ratio of initial anode capacity to initial cathode capacity	1.1
R	radius of the spherical electrode particle (m)	5×10^{-6} (m)
$\varepsilon_{1\alpha}$	solid phase porosity of the electrode film	0.65
η_1	formation cycle efficiency	0.9
ρ_{cr}	number of cracks per unit area of the particle (m^{-2})	2.54×10^{18} (m^{-2})
ρ_{SEI}	density of SEI films (gm m^{-3})	2.11×10^6 $(gm\ m^{-3})$
Ω	partial molar volume of the solute (m^3 mol^{-1})	$8.9 * 10^{-6}$ $(m^3\ mol^{-1})$
–	Specific capacity of graphite (mAh gm^{-1})	339 $(mAh\ gm^{-1})$

References

1. M. Winter, J. O. Besenhard, M. E. Spahr, and P. Novak, *Adv. Mater.*, **10**(10), 725 (1998).
2. D. Aurbach, *Journal of Power Sources*, **89**(2), 206 (2000).
3. M. Wachtler, J. O. Besenhard, and M. Winter, *Journal of Power Sources*, **94**(2), 189 (2001).
4. E. Markervich, G. Salitra, M. Levi, and D. Aurbach, *Journa of Power Sources*, **146**, 146 (2005).
5. J. Yan, B.-J. Xia, Y.-C. Su, X.-Z. Zhou, J. Zhang, and X.-G. Zhang, *Electrochimica Acta*, **53**(24), 7069 (2008).
6. R. Spotnitz, *Journal of Power Sources*, **113**(1), 72 (2003).
7. I. Bloom, B. W. Cole, J. J. Sohn, S. A. Jones, E. G. Polzin, V. S. Battaglia, G. L. Henriksen, C. Motloch, R. Richardson, T. Unkelhaeuser, D. Ingersoll, and H. L. Case, *Journal of Power Sources*, **101**(2), 238 (2001).
8. J. Christensen and J. Newman, *Journal of The Electrochemical Society*, **151**(11), A1977 (2004).
9. M. Safari, M. Morcrette, A. Teyssot, and C. Delacourt, *Journal of The Electrochemical Society*, **157**(6), A713 (2010).
10. M. Safari, M. Morcrette, A. Teyssot, and C. Delacourt, *Journal of The Electrochemical Society*, **157**(7), A892 (2010).
11. Q. Zhang and R. E. White, *Journal of Power Sources*, **173**(2), 990 (2007).
12. Q. Zhang and R. E. White, *Journal of Power Sources*, **179**(2), 785 (2008).
13. Q. Zhang and R. E. White, *Journal of Power Sources*, **179**(2), 793 (2008).
14. R. P. Ramasamy, R. E. White, and B. N. Popov, *Journal of Power Sources*, **141**(2), 298 (2005).
15. R. P. Ramasamy, J.-W. Lee, and B. N. Popov, *Journal of Power Sources*, **166**(1), 266 (2007).
16. M. Broussely, P. Biensan, F. Bonhomme, P. Blanchard, S. Herreyre, K. Nechev, and R. J. Staniewicz, *Journal of Power Sources*, **146**(1–2), 90 (2005).
17. G. Ning, R. E. White, and B. N. Popov, *Electrochimica Acta*, **51**(10), 2012 (2006).
18. K. Kumaresan, Q. Z. Guo, P. Ramadass, and R. E. White, *Journal of Power Sources*, **158**(1), 679 (2006).
19. S. Santhanagopalan, Q. Guo, P. Ramadass, and R. E. White, *Journal of Power Sources*, **156**(2), 620 (2006).
20. J. Christensen and J. Newman, *Journal of The Electrochemical Society*, **153**(6), A1019 (2006).
21. J. Christensen and J. Newman, *Journal of Solid State Electrochemistry*, **10**(5), 293 (2006).
22. X. Zhang, A. M. Sastry, and W. Shyy, *Journal of The Electrochemical Society*, **155**(7), A542 (2008).
23. X. Zhang, W. Shyy, and A. M. Sastry, *Journal of The Electrochemical Society*, **154**(10), A910 (2007).
24. V. A. Sethuraman, N. Van Winkle, D. P. Abraham, A. F. Bower, and P. R. Guduru, *Journal of Power Sources*, **206**, 334 (2012).
25. R. Deshpande, Y.-T. Cheng, and M. W. Verbrugge, *Journal of Power Sources*, **195**(15), 5081 (2010).
26. R. Deshpande, Y. Qi, and Y.-T. Cheng, *Journal of The Electrochemical Society*, **157**(8), A967 (2010).
27. S. J. Harris, R. D. Deshpande, Y. Qi, I. Dutta, and Y. T. Cheng, *J. Mater. Res.*, **25**(8), 1433 (2010).
28. R. Deshpande, Y.-T. Cheng, M. W. Verbrugge, and A. Timmons, *Journal of The Electrochemical Society*, **158**(5), 1 (2011).
29. Y.-T. Cheng and M. W. Verbrugge, *Journal of Applied Physics*, **104**(8), 083521 (2008).
30. A. K. Padhi, K. S. Nanjundaswamy, and J. B. Goodenough, *Journal of the Electrochemical Society*, **144**(4), 1188 (1997).
31. N. Ravet, Y. Chouinard, J. F. Magnan, S. Besner, M. Gauthier, and M. Armand, *Journal of Power Sources*, **97-98**, 503 (2001).
32. N. Recham, L. Dupont, M. Courty, K. Djellab, D. Larcher, M. Armand, and J. M. Tarascon, *Chem. Mat.*, **21**(6), 1096 (2009).
33. B. Kang and G. Ceder, *Nature*, **458**(7235), 190 (2009).
34. S. Y. Chung, J. T. Bloking, and Y. M. Chiang, *Nature Materials*, **1**(2), 123 (2002).
35. P. Liu, J. Wang, J. Hicks-Garner, E. Sherman, S. Soukiazian, M. Verbrugge, H. Tataria, J. Musser, and P. Finamore, *J. Electrochem. Soc.*, **157**(4), A499 (2010).
36. J. Wang, P. Liu, J. Hicks-Garner, E. Sherman, S. Soukiazian, M. Verbrugge, H. Tataria, J. Musser, and P. Finamore, *Journal of Power Sources*, **196**(8), 3942 (2011).
37. M. W. Verbrugge and B. J. Koch, *Journal of The Electrochemical Society*, **150**(3), A374 (2003).
38. R. A. Huggins, *Advanced Batteries: Materials Science Aspects*. (Springer, 2009).
39. Y.-T. Cheng and M. W. Verbrugge, *Journal of Power Sources*, **190**(2), 453 (2009).
40. P. C. Paris and F. Erdogan, *Journal of basic engineering*, **84**(4), 528 (1963).
41. S. Suresh, *Fatigue of Materials,* second ed. (Cambridge, 1998).
42. B. Lawn, *Fracture of brittle solids*, second ed. (Cambridge university press, United Kingom, 1993).
43. T. L. Anderson, *Fracture Mechancis – Fundamentals and Applications* third ed. (Taylor and Francis, Boca ranton, FL- 33487, 2005).
44. L. Y. Beaulieu, K. W. Eberman, R. L. Turner, L. J. Krause, and J. R. Dahn, *Electrochem. Solid State Lett.*, **4**(9), A137 (2001).
45. A. R. Ragab and S. B. Bayoumi, *Engineering Solid Mechanics- Fundamental and Applications*. (CRC Press, Boca Ranton, FL, 1999).
46. H. D. Solomon, G. R. Halford, L. R. Kaisand, and B. N. Leis, *Low Cycle Fatigue*. (Symposium proceedings volume, ASTM, Philadelphia, PA, 1987).
47. H. E. Boyer, *Atlas of Fatigue Curves*. (American Society for Metals, Metals Park, OH 1986).
48. Y. Qi, H. Guo, J. L. G. Hector, and A. Timmons, *Journal of The Electrochemical Society*, **157**(5), A558 (2010).
49. M. D. Levi and D. Aurbach, *Journal of Physical Chemistry B*, **101**(23), 4641 (1997).